Received: 21 November 2021 | Revised: 31 December 2021 | Accepted: 13 January 2022

DOI: 10.1002/agt2.173

Aggregate WILEY

RESEARCH ARTICLE

Solid-phase molecular self-assembly facilitated supramolecular films with alternative hydrophobic/hydrophilic domains for skin moisture detection

Jinwan Qi | **Tongyue Wu** | **Wenkai Wang** | **Hongjun Jin** | **Shuitao Gao** | **Shasha Jiang** | **Jianbin Huang** | **Yun Yan**

Beijing National Laboratory for Molecular Sciences (BNLMS), College of Chemistry and Molecular Engineering, Peking University, Beijing, China

Correspondence
Yun Yan, Beijing National Laboratory for Molecular Sciences (BNLMS), College of Chemistry and Molecular Engineering, Peking University, Beijing 100871, China.
Email: yunyan@pku.edu.cn

Funding information
National Natural Science Foundation of China, Grant/Award Numbers: 22172004, 91856120, 21972003

Abstract

Human skin moisture is closely related to health and personal care issues. Many creams were developed to claim capable of skin moisturizing. However, people can hardly check their skin moisture status and the moisturizing effect of various creams conveniently, since currently all the skin moisturizing detection rely on large equipment requiring power supply. Herein, we report a power-supply independent supramolecular film that is able to directly report the moisturizing status of the skin. With the strategy of solid-phase molecular self-assembly (SPMSA), the aqueous precipitates formed by commercially available polyelectrolyte and oppositely charged surfactant would transform into a supramolecular film under a mild mechanical pressure, where the hydrophobic surfactant domains bridged by polyelectrolyte merge into hydrophobic mesophases to reduce interfacial energy. The hydrophobic mesophase will greatly retard water diffusion inside the film, so that a humidity gradient is generated as the film is exposed to a humid environment. The film will bend upward automatically in touch with moisture skin, and the bending degree is proportional to the skin moisture status. Therefore, the film can be used as portable smart power-free skin moisture sensor.

KEYWORDS
bilayer, solid-phase molecular self-assembly, suppramolcular films

1 | INTRODUCTION

The level of water content in living organisms is of crucial importance for their health. The water content of the skin is not only one of the most important parameters of skin condition, but also a vital indicator of human health.[1–3] With the development of bioengineering applications followed by the dermatocosmetic research, the moisture information on skin such as the water content and the water barrier function attracted increasing attention. To measure the skin properties objectively, several techniques have been developed such as the optical coherence tomography,[4] confocal Raman spectroscopy,[5] microfluidic channels,[6] and electrodermal tests.[7–9] And up to now, a few of commercially available instruments are also used for skin moisture detection in dermatocosmetic research.

Despite the significant progress, these methods always need relatively large equipment with tedious and complicated fabrication or need to be connected to an external power supply, which is not energy-favorable and not convenient for daily use. We report herein a simple and efficient one-pot bottom-up approach to create a supramolecular skin moisture sensory film capable of reporting the skin moisture status without the requirements of power supply. The film was made through a pressing-facilitated solid-phase molecular self-assembly (SPMSA) approach recently developed by us.[10,11] A precipitate composed of oppositely charged polyelectrolyte (PE) and surfactant was first generated in water, which would immediately transform into a free-standing supramolecular film under a mild mechanical pressure owing to the merging of the surfactant domains. This free-standing film has excellent hygroscopicity, but water evaporation or absorption on the surface is much faster than the water diffusion in its interior owing to the presence of hydrophobic domains (Scheme 1). As a result, when the surface is quickly "hydrated" or "dried" in respond to environmental humidity,

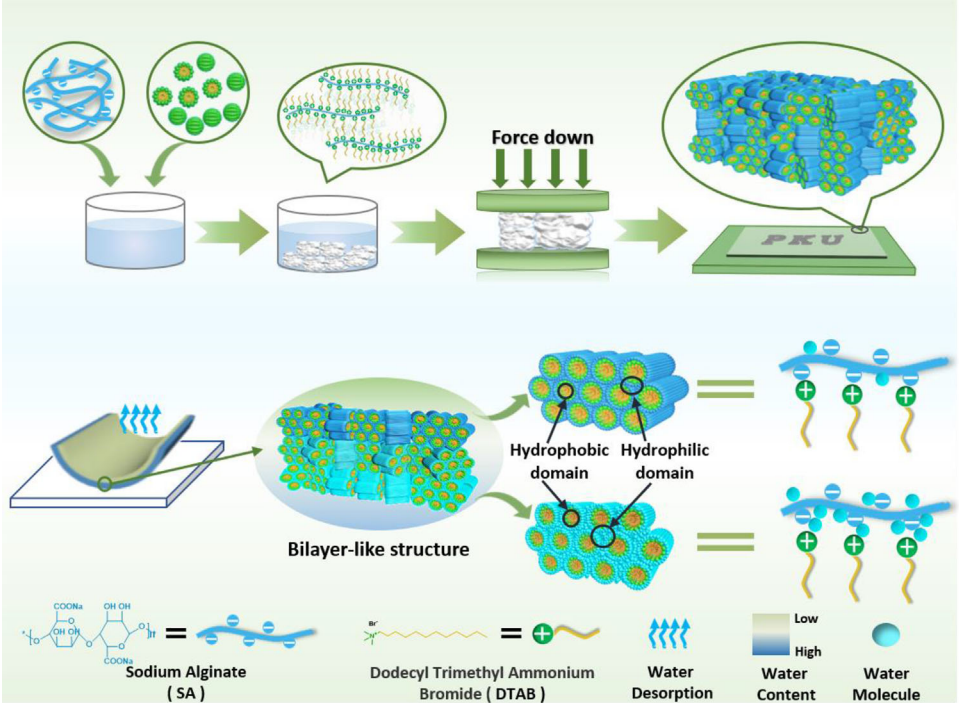

SCHEME 1 Schematic illustration of the fabrication procedure of the film and the mechanism of moisture-driven actuation

there would be a retarded humidity response in the interior. This humidity gradient yields mechanical responses to drive the film bending. Strikingly, the film bending is so sensitive to external moisture, it would bend immediately against an approaching finger, remotely without direct touching and returns to its original flat state in similar time scale as the finger moved away. Since the amplitude of the mechanical response is directly related with the skin moisture condition, this supramolecular film can be used as a portable power-free skin moisture sensor. The simple fabrication methods, the renewable and commercial resources and the possibility of industrial-scale production, prove its desirable application prospections.

2 | EXPERIMENTAL SECTION

2.1 | Materials and chemicals

N, N, N-trimethyl-1-dodecanaminium bromide (DTAB) was purchased from Macklin Corporation. Sodium alginate was purchased from Beijing Tong Guang Fine Chemicals Company. Carboxymethylcellulose sodium (CMC) was purchased from Tianjin Guangfu Fine Chemical Research Institute and polydimethyl diallyl ammonium chloride (PDDA, $M_w \sim$ 400,000) was purchased from Sigma-Aldrich Corporation. The aqueous solutions were prepared by using Milli-Q water of 18 MΩ. All the reagents were of AR grade and used as received without further purification.

2.2 | Experimental design

An aqueous solution of DTAB (50 mM) was added to an aqueous solution of SA (50 mM), to reach final concentrations of 25 mM for both the carboxylate negative charges of SA and the ammonium positive charges of DTAB. After mixing, the white precipitates were separated from the suspensions by centrifugation with a speed of 5000-8000 rpm. The collected precipitates were then pressed by finger, bottle rolling, or noodle machine manufacturing under ambient environment to get transparent plastic films.

2.3 | Film-bending characterization

The bending of the film was monitored using a video camera, and the deflection angle $\theta°$ was measured as described in the inset of Figure 2C. Different humidity conditions are achieved by adding saturated aqueous solutions of different inorganic salts to well-sealed desiccators (Supplementary Table S4 and Figure S7); the actual humidity is measured by a commercially available hygrometer.

2.4 | Other characterizations

The weight ratios of C, N, and H were collected from a EL elemental analyzer (Elementar Analysensysteme GmbH). X-ray diffraction (XRD) measurements were performed using a Rigaku Dmax-2400 diffractometer with Cu Kα radiation. The fresh precipitates were freeze-dried at -50°C for the XRD measurement after being separated from the suspensions by centrifugation. The lamellar period d in each sample was calculated using Bragg's Law, where $d = \lambda / 2\sin\theta$. The particle size D in each sample was estimated using Scherrer Equation, where $D = K\lambda / (B\text{-}B') \cos\theta$. Herein, K is a constant taken as 0.89, while B is the full width at half maximum (FWHM) of the sample's scattering peak at the diffraction angle θ and B' is the FWHM of the standard's scattering peak, which is 0.10°. In this study, the strongest peak corresponding to d_1 was taken for calculation. Other characterizations including polar optical microscope (POM) picture, Fourier transform infrared (FT-IR) spectra, TGA experiments, differential

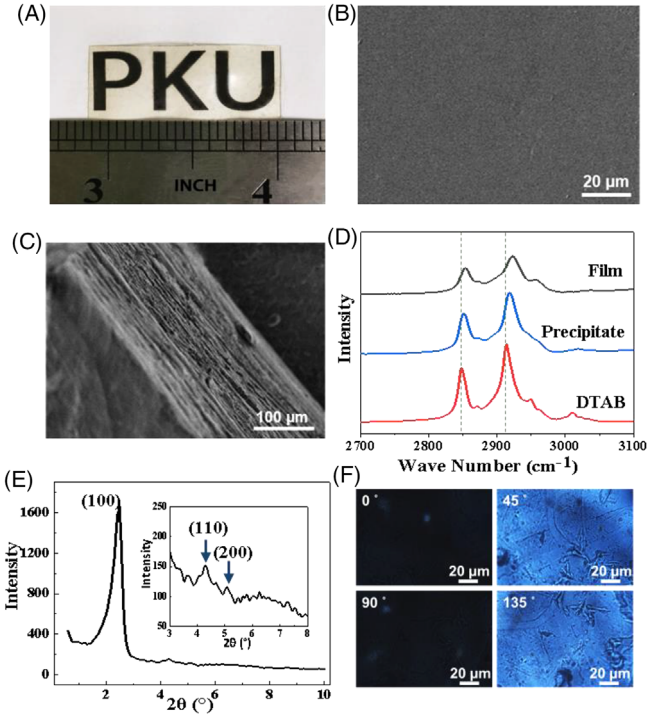

FIGURE 1 Structure and characterization of the SA-DTAB films. (A) Photo of the transparent film. (B) SEM image of the surface. (C) SEM image of the cross section. (D) ATR-IR spectra of the SA, DTAB, SA-DTAB precipitate, and SA-DTAB film. Shifting peaks are indicated by dashed lines. (E) XRD pattern of the film. (F) POM image of the film at different angles

scanning calorimetry (DSC) experiments, scanning electron microscopy (SEM) measurements, atomic force microscopy (AFM) measurements, and mechanical properties were performed similarly as illustrated in our work before.[10]

3 | RESULTS

3.1 | Basic composition and structure

The oppositely charged surfactant and polyelectrolyte in this study is the commercially available N, N, N-trimethyl-1-dodecanaminium bromide (DTAB) and sodium alginate (SA) (Scheme 1). When dissolved in water, DTAB tends to self-assemble into spherical micelles at concentrations above 15 mmol/L. White precipitates occurred upon mixing with SA solution at charge balancing ratio. After centrifugation under 5000–8000 rpm, the precipitate was separated and collected. If no external force is applied, the dispersed precipitate will form a translucent block after 24 h, and the incomplete fusion of the particles inside the block will cause a large number of defects. When the auxiliary pressure is applied, such as a pressure exerted by a human figure, about 50 KPa, the precipitate will immediately transform into a continuous cake, which becomes a transparent film within 2 h under a relative humidity (RH) of 20% (Figure 1A). The film formation will be complete within 15 min as the RH is as high as 100%. Massive generation of the film with controlled film thickness is possible using a roller-type noodle machine.[10,11] The film has good processibility, and its surface is very smooth under SEM (Figure 1B). AFM measurement revealed a roughness $Ra \approx 9.48$ nm (Figure S1). The SEM image of the film's cross section (Figure 1C) indicated a lamellar structure in the film at mesoscope scale. The disordered small surfactant domains in the precipitates might have transformed into liquid crystalline mesophases under mechanical pressure, which reduced the domain boundaries to form the bulk film. Elemental analysis manifested that the film is charge-neutral with a 1:1 composition of the DTAB cations and alginate polyanions (Table S1). Meanwhile, thermal gravimetric analysis (TGA) combined with Element Analysis suggested that each pair of the unit on average binds 2.3 water molecules (Table S1 and Figure S2). DSC results showed no signal ice melting between 0°C and -80°C, indicating that these water molecules are not sufficient enough to form an independent phase(Figure S3), which simply bound physically to the ionic groups in the film.[12] These water molecules are crucial for the film formation since they endow the polyions and surfactant molecules with the ability of rearrangement in the solid phase. Figure 1D shows that the symmetric and antisymmetric vibrations of the C-H bond for the alkyl chain of DTAB in the film occur at the higher wavenumber of 2852 cm^{-1} and 2923 cm^{-1}, whereas those in the amorphous precipitate decrease to 2850 cm^{-1} and 2918 cm^{-1} (Table S2). Since the larger wavenumbers indicate less ordered alkyl chain packing,[13] this result manifests that the DTAB molecules in each of the clusters in the precipitates have migrated to the neighboring clusters to form an entire film. Because these processes occurred in solid phase, the DTAB molecules cannot migrate as freely as those in solution, the resultant chain packing in the film becomes less order.

The XRD pattern of the fresh precipitates, after freeze-drying, gives only one diffraction in the low-angle region (Figure S4A) and the corresponding distance is 3.36 nm. This is nearly the extending length of two DTAB molecules (3.06 nm), indicating the presence of ordered bilayer domains of the surfactant in the precipitates. The 0.30 nm larger distance indicates that the SA chains have folded on the polar surface of DTAB bilayers via electrostatic interactions (Figure S4C). Notably, this diffraction is significantly sharpened and intensified after the precipitates were pressed into a film (Figure 1E). Furthermore, two extra weak diffractions appeared. All these three diffractions met a spacing ratio of 1: $\sqrt{3}$: 2, characterizing (100), (110), and (200) Miller Indices of a 2D hexagonal mesostructure.[14] The corresponding lattice parameter, a, is 4.1 nm,[15] where $a = 4\pi\frac{\sqrt{h^2+k^2+hk}}{\sqrt{3}q_{hkl}}$. Besides, the XPS spectra (N 1s) of the SA-DTAB film and DTAB (Figure S4D) indicated the electrostatic interaction between the DTAB and SA molecules. This means that the DTAB molecules, which are electrostatically bonded to the SA chains, self-assembled into wormlike micelles, and packed further into hexagonal phases.[16] According to the Scherrer equation,[17] the average size of the DTAB hexagonal domain in the film is about 500–600 nm (Figure 3D and Table S3) in different humidity environment. This large size is comparable to the wavelength of visible light, so that the film shows significant birefringence (Figure 1F).

3.2 | Moisture-responding behavior

The resultant film displays humidity sensitive motion ability. Figure 2A shows that the film would bend immediately

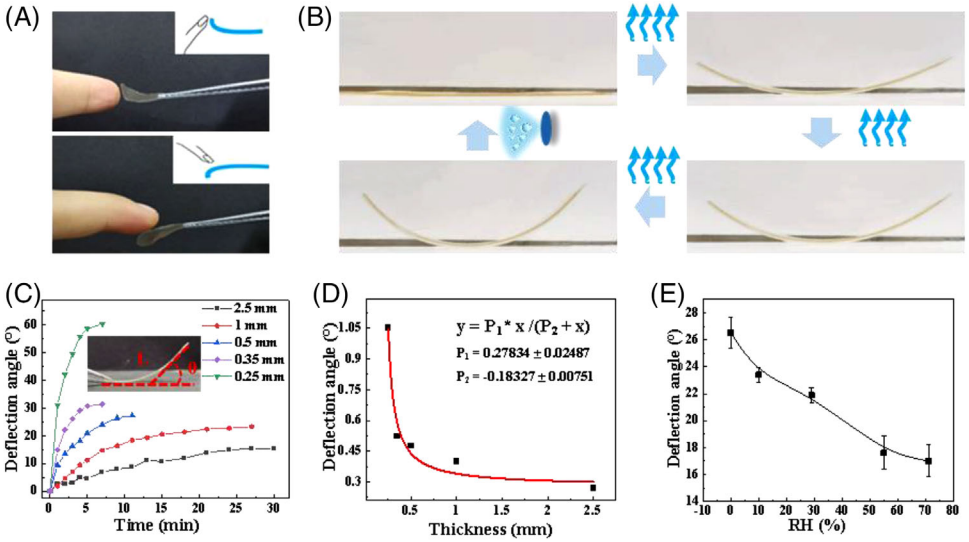

FIGURE 2 Performance of the SA-DTAB film actuator. (A) Photos of the film bending against an approaching finger at a distance of a few millimeters. (B) The reversible bending behavior of the SA-DTAB film. (C) Variation of the extent of bending (deflection angle) with time for the films with different thickness. The relative humidity (RH) of environment is 10%. (D) The dependence of the maximum deflection angle with the thickness of the film (RH = 10%). (E) Variation of the deflection angle with increased humidity for a 0.5 mm thick film

against an approaching finger, remotely without direct touching. The film returns to its original flat state in similar time scale as the finger moved away, indicating that the bending is reversible (Movie 1–2). As the film moved toward a humidifier, it bent backward and reached a steady-state rapidly, typically within 40 s (Movie 3). Upon transferring the film on a glass slide from the high-humidity environment to the low one, it spontaneously bent upward in tens of seconds, and recovered to the original flat state when a humidifier was approached from the bending direction (Figure 2B).

Next, the deflection angle θ (inset in Figure 2C) was quantitatively monitored using a video camera. We first investigated the effect of the thicknesses of the film on the deflection angle. Figure 2C shows that at a fixed relative humidity RH = 10%, only thin films display considerable deflection with high bending speed. A 0.25 mm thick film would bend upward with the angle of 58.61° within 5 min, whereas a 1 mm thick film can only bend 11.21° at the same time scale. As the film thickness is increased to 2.5 mm, the bending was negligible. The deflection angle as a function of the film thickness gives a hyperbola correlation (Figure 2D), suggesting that the film's locomotion could be regulated by controlling its thickness. The bending ability of the film decreases with increasing environmental humidity. For a 0.5 mm thick film, the deflection angle after 5 min is about 26.5° at RH = 0, whereas it gradually decreases to 17.01° at RH = 71% (Figure 2E), indicating that the film is able to response to different humidity gradient.

3.3 | Mechanism of the moisture-driven film bending

The moisture-driven bending is closely related to the faster water exchange on the surface than water diffusion inside the film. The progress of water adsorption onto the surface was monitored in situ with attenuated total reflection infrared spectroscopy. The film was placed in a desiccator saturated with deuterium water(D_2O). As the film exchanged moisture with the environment, the $\nu_{(OD)}$ band on surface at 2500 cm^{-1} increased rapidly, which was accompanied by concomitant decrease of the $\nu_{(OH)}$ band at 3000 cm^{-1}. This process would reach saturation within 120 s (Figure 3A). However, the weight of the film would become constant at least 5 h later (Figure 3B). This means that the adsorption of water molecules on the surface of the film is much faster than their diffusion inside the film, which generates humidity gradient in the film. Noticeably, compared with the slow water-acquiring rate, the water loss from the film is so fast that nearly 90 % of the acquired water was lost within 1 h, as revealed by the right panel in Figure 3B. Furthermore, the water loss from the upper surface is also much faster than that from the lower one. As an evidence, the vibrational band at 2500 cm^{-1} for the upper surface of a D_2O saturated film is much weaker than that for the lower surface (Figure 3C).

XRD measurements would explain the impact of the asymmetric humidity distribution inside the film on its actuation performance. Figure 3D reveals that with increasing the environmental humidity from 0% to 70%, the (001) diffraction shift to lower angles, and the corresponding interlayer spacing of the film increases from 3.34 to 3.56 nm. This is because the water molecules have entered the hydrophilic layers of the hexagonal phase (Figure 3D and Table S3), which increases the interlayer spacing.[10] This is exactly the scenarios occurred in the process of water absorption/ evaporation in the film. The humidity gradient generated in the process of water gain or loss in the film would result in a consequent gradient of internal interlayer spacing, which drove the asymmetric film deformation and locomotion. In this way, the film behaved like a pseudo bilayer structure. As illustrated in Figure 3E, the upper surfaces contracts significantly due to the fast water loss, so that upward deformation of the film occurs.

The slower diffusion rate of water molecules inside the film can be attributed to the coexistence of hydrophobic mesophases with hydrophilic shells, which hampers the continuous diffusion of water inside the membrane (Table 1). As a control, the cationic surfactant DTAB was replaced with

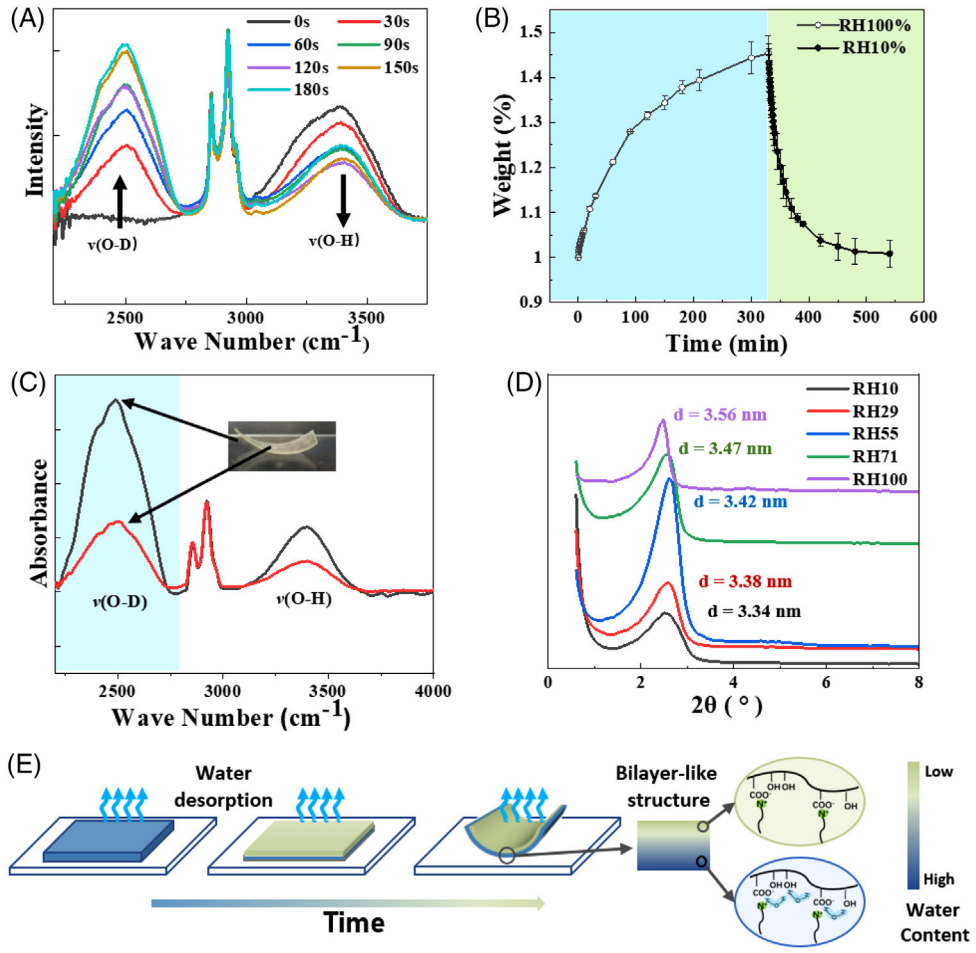

FIGURE 3 Mechanism of the SA-DTAB film actuator. (A) Time-dependent ATR–IR spectra of the film by placing the film in D_2O-saturated environment. (B) Weight variation of the film with relative humidity of the environment. (C) ATR-IR spectra of the upper and lower surface of the film, showing that the upper surface undergoes faster of D_2O loss than the lower one. (D) XRD patterns of the film in different relative humidity environment. (E) Schematic of the pseudo bilayer structure of the film

TABLE 1 Role of hydrophobic domains on the bending ability of the film

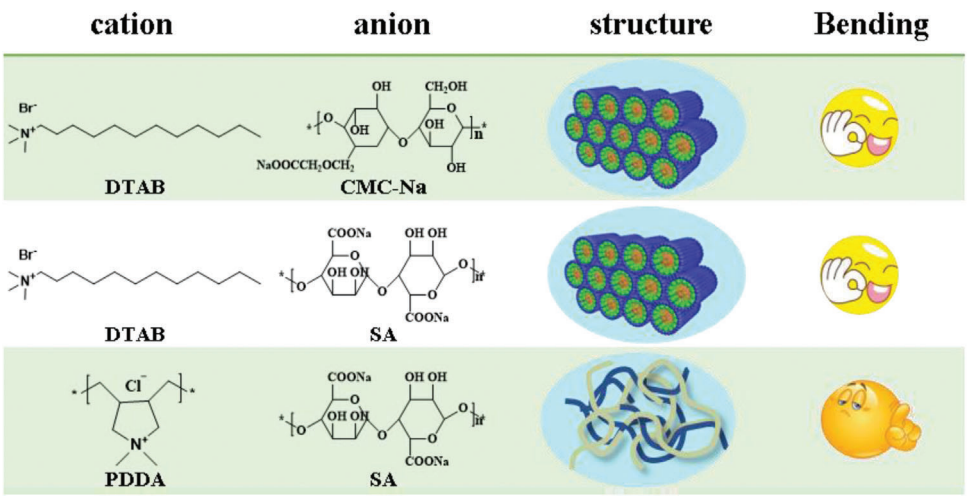

the cationic polyelectrolyte-polydimethyl diallyl ammonium chloride (PDDA) to prepare a film with the same method. The resultant film is composed of physically entangled chains of PDDA and SA, where no distinct hydrophobic mesophases could form (Figure S4B). Actually, no such actuating performance for the large variety of polymeric composite films.[18] The water absorption and evaporation curves of the film over time are almost linear (Figure S5), indicating similar water diffusion rate on the surface and inside the film. Accordingly, the film does not response to humidity gradients. In contrast, as we keep DTAB but use the negatively charged carboxymethylcellulose sodium (CMC) to replace SA, the

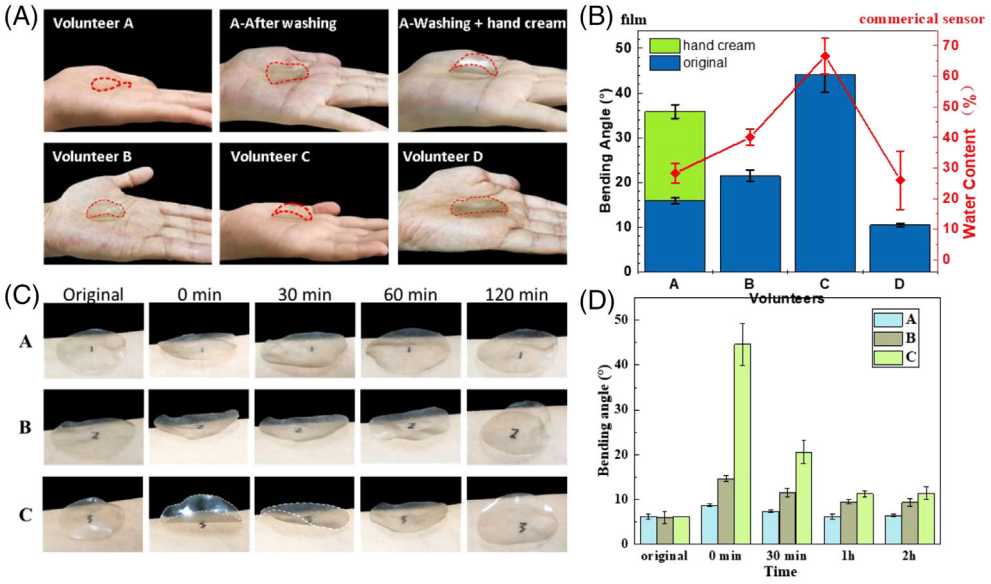

FIGURE 4 The skin moisture sensitivity of the film under different conditions. (A, B) The skin moisture sensitivity of the film under different volunteers. The capital in each picture refers to different volunteers. (C, D) The skin moisture sensitivity of the film after using different skin protecting cream. A–C are film deformation status after cream A, B, and C are applied. It is clear that cream A did not have sufficient moisture, while cream C is capable provide moisture environment for skin even after applying for 2 h

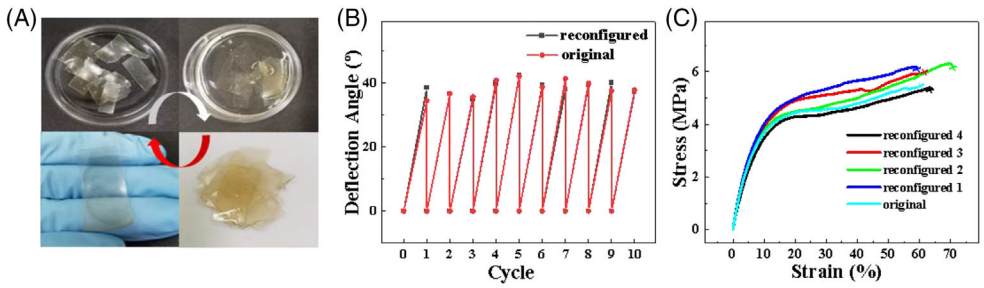

FIGURE 5 (A) The film regeneration process at room temperature. (B) The maximum bending angle of Figure 4B and the film thickness is 0.35 mm and RH = 10%. (C) Stress–strain curves of the SA-DTAB films underwent different numbers of reconfiguration cycles

resultant film, with the same hexagonal phase structure inside (Figure S4B), displayed similar humidity responsive performance (Figure S6).

3.4 | Application of the film

The humidity triggered deformation of the film makes it an excellent power-free skin moisture detection sensor. Different from other skin moisture status sensing based on circuit-based instruments, the current film would report the skin moisture status directly with its bending extent. Figure 4A and B shows the film bending status on different volunteers. We invited four volunteers A, B, C, and D, corresponding to 30-year-old female, 30-year-old male, 25-year-old female, and 10-year-old boy, respectively. The results showed that the bending degree of the films on the palms of different volunteers was different, reflecting the differences in their palm moisture. It is clear that the film on the palm of volunteer C bends most strikingly, whereas that for volunteer A is the slightest. The red line in Figure 4B shows the water content of these volunteers obtained with a commercial equipment, which gives the similar trends to the reports provided by the current DTAB-SA film, indicating the current supramolecular sensor displayed satisficed reliability (Figure 4B).

Furthermore, if the skin was protected with hand cream, this film can be used to test the water retention property of different creams (Figure 4C and D). To ensure the skin is large enough to apply three different hand creams, we choose the arm skin (of volunteer A) for test. The arm was washed before the creams A, B, and C were applied. Figure 4C shows the status of film bending on these creams in 0 min, 30 min, 1 h, and 2 h. The bending angle of the film on the hand cream-treated skin all increases to varying extent. Among them, the moisturizing ability of hand cream A is almost negligible. The moisturizing effect of hand cream B is relatively stable, indicating this hand cream has stable water retention ability. Hand cream C has the highest initial water retention ability, but the content of water decreases within 2 h. However, this reduced water retention is still nearly the same as that of hand cream B, suggesting hand cream C has the best moisturizing effect. The above results show the possibility of the current sensory film as a portable skin moisture detector.

3.5 | Regeneration ability of the film

The bending ability of the film remained stable after ten cycles of use (Figure 5B). Actually, due to the noncovalent

nature of the film, this SA-DTAB film could be rejuvenated over and over again, regardless of what damage it incurred. Figure 5A shows that after wetting with water, we can easily knead the fragments together and press to regenerate a fresh new film. The renewed film exhibited the same structure as the original one (Figure S8). Compared with the original one, both the bending ability (Figure 5B) and the mechanical strength of the rejuvenated SA-DTAB film were not affected noticeably (Figure 5C). Since the sensory film would inevitably encourage damage, the current study demonstrated an efficient approach to create a structural sensor with long service life.

4 | CONCLUSION

In conclusion, we report the generation of a supramolecular film displaying skin moisture sensitive bending ability via the strategy of solid-phase molecular self-assembly (SPMSA). Upon mechanically pressed precipitates of oppositely charged commercial surfactant and polyelectrolyte, a supramolecular film with alternatively arranged hydrophobic/hydrophilic domains can be created. This structural feature retarded the diffusion of water inside the film, which resulted in different interlayer spacings in different depths of the film. As a result, the film would bend as it exchanges water with environment. In this way, we are able to create a portable power-free skin moisture sensor for skin status detection. We envision that the SPMSA would be a general strategy to create smart materials.

ACKNOWLEDGMENTS

This work was supported by the National Natural Science Foundation of China (NSFC 22172004, 91856120, and 21972003)

AUTHOR CONTRIBUTIONS

J. Q. designed the research, conducted most of the experiments, and wrote up the draft paper; S. G. helped to conduct the mechanical characterization; T. W. and W. W. helped to perform the XRD, ATR-IR, and AFM experiments; H. J. helped to perform the TGA and DSC tests; J. Q., Y. Y., W. W., S. J., and J. H. analyzed the data; Y. Y. supervised the research at all the stages and revised the manuscript.

CONFLICT OF INTEREST

The authors declare no conflict of interest.

DATA AVAILABILITY STATEMENT

The data that support the findings of this study are available from the corresponding author upon reasonable request.

ORCID

Jinwan Qi https://orcid.org/0000-0001-7180-9868
Yun Yan https://orcid.org/0000-0001-8759-3918

REFERENCES

1. W. J. A. Meuling, A. C. Franssen, D. H. Brouwer, J. J. V. Hemmen, *Sci. Total Environ.* **1997**, *199*, 165.
2. G. Yosipovitch, E. Tur, O. Cohen, Y. Rusecki, *Diabetes Care* **1993**, *16*, 560.
3. G. Yosipovitch, E. Tur, G. Morduchowicz, G. Boner, *Nephrol. Dial. Transplant.* **1993**, *8*, 1129.
4. C.-K. Lee, M.-T. Tsai, F.-Y. Chang, C.-H. Yang, S.-C. Shen, O. Yuan, C.-H. Yang, *Sensors* **2013**, *13*, 4041.
5. N. Nakagawa, M. Matsumoto, S. Sakai, *Skin Res. Technol.* **2010**, *16*, 137.
6. M. Bariya, H. Y. Y. Nyein, A. Javey, *Nat. Electron.* **2018**, *1*, 160.
7. Y. Wang, L. Zhang, J. Zhou, A. Lu, *ACS Appl. Mater. Inter.* **2020**, *12*, 7631.
8. Y. Lu, Y. Fujita, S. Honda, S.-H. Yang, Y. Xuan, K. Xu, T. Arie, S. Akita, K. Takei, *Adv. Healthc. Mater.* **2021**, *10*, 2100103.
9. T.-H. Huang, J.-C. Chou, T.-P. Sun, S.-K. Hsiung, *Sensor. Actuat. B-Chem.* **2008**, *134*, 206.
10. H. Jin, M. Xie, W. Wang, L. Jiang, W. Chang, Y. Sun, L. Xu, S. Zang, J. Huang, Y. Yan, L. Jiang, *CCS Chem.* **2020**, *2*, 98.
11. W. Wang, M. Xie, H. Jin, W. Zhi, K. Liu, C. Ma, P. Liao, J. Huang, Y. Yan, *Mater. Chem. Front.* **2020**, *4*, 1530.
12. P. Batys, Y. Zhang, J. L. Lutkenhaus, M. Sammalkorpi, *Macromolecules* **2018**, *51*, 8268.
13. Y. Yan, W. Xiong, J. Huang, Z. Li, X. Li, N. Li, H. Fu, *J. Phys. Chem. B* **2005**, *109*, 357.
14. C. K. Ober, G. Wegner, *Adv. Mater.* **1997**, *9*, 17.
15. S. Koga, S. Mann, *J. Mater. Chem.* **2010**, *20*, 5736.
16. F. Yeh, E. L. Sokolov, A. R. Khokhlov, B. Chu, *J. Am. Chem. Soc.* **1996**, *118*, 6615.
17. M. Xie, Y. Che, K. Liu, L. Jiang, L. Xu, R. Xue, J. Huang, M. Drechsler, B. Z. Tang, Y. Yan, *Adv. Funct. Mater.* **2018**, *28*, 1803370.
18. X. Liu, J. Sun, *Aggregate*. **2021**, *2*, e109.

SUPPORTING INFORMATION

Additional supporting information may be found in the online version of the article at the publisher's website.

How to cite this article: J. Qi, T. Wu, W. Wang, H. Jin, S. Gao, S. Jiang, J. Huang, Y. Yan, *Aggregate* **2022**, e2173. https://doi.org/10.1002/agt2.173